Journal of Physics: Conference Series **88** (2007) 012006 doi:10.1088/1742-6596/88/1/012006

Photo-Double Ionization of H_2

M Gisselbrecht[1], M Lavollée[1], A Huetz[1], P Bolognesi[2], L Avaldi[2], D P Seccombe[3], and T J Reddish[3]

[1] CNRS;Univ Paris-Sud, LIXAM UMR 8624, Bât 350, Orsay Cedex, F-91405, France
[2] CNR -IMIP Area della Ricerca di Roma 1, CP 10 00016 Monterotondo Scalo, Italy.
[3] Department of Physics, University of Windsor, 401 Sunset Ave, Ontario, Canada, N9B 3P4

E-mail: mathieu.gisselbrecht@u-psud.fr

Abstract. The Coulomb explosion of the hydrogen molecule, after absorption of a 76 eV photon, has been studied by momentum imaging the two electrons and the two protons. Absolute fully differential cross sections (FDCS) are compared with Time Dependent Close Coupling (TDCC) calculations and the first-order helium-like model in the coplanar geometry for equal electron energy sharing. While the helium-like model gives a consistent agreement in shape and magnitude with experimental data, the comparison with the TDCC calculations highlights the limit of this model when the molecular axis' orientation is along the polarization direction. New evidence of changes in the FDCS with internuclear separation is reported for the coplanar geometry.

1. Introduction

Photo-double ionization (PDI) of atoms and molecules by a single photon is a manifestation of the electron-electron interaction in both initial and final states of the investigated system. Indeed in the independent particle description of photo-absorption, a photon interacts with no more than one electron (dipole-operator) and cannot lead to the simultaneous ejection of two electrons.

PDI of the simplest two-electron molecule, hydrogen, has attracted significant interest [1-15] as it provides a prototypal system to obtain physical insight into the 4-body problem. PDI of H_2 is followed by a 'Coulomb explosion' of the resulting two bare protons. For excess energies greater than a few eV, the *axial recoil approximation* [16] is considered valid since electron ejection is instantaneous and the protons 'explode' apart rapidly (~fs) compared to molecular rotation (~ps). Consequently, the relative momentum of the two escaping protons defines the molecular alignment at the instant of photo-fragmentation.

Experimental techniques have been steadily improving enabling studies of the correlated electron pair dynamics produced in PDI [17]. More recently, energy and angle-resolved detection of *all* four particles has become feasible [1-3] on H_2/D_2. This, combined with a well-defined light polarisation state, completely defines the PDI dynamics and allows the study of the fully differential cross sections (FDCSs) within the *molecular* frame using so-called 'fixed-in space' molecules.

The FDCSs of H_2 are significantly more complex than in helium and introduce new physical effects. The single-centre expansion approaches by Feagin and Reddish [4, 5] - called the helium-like model (HeL) in the following - and Kheifets and Bray [6, 7] have been successful in the case of partially differential cross sections in equal energy sharing conditions. We have recently studied the

limits of the HeL approach in describing the FDCSs [3]. The general consequences of the optical selection rules for aligned, or 'fixed-in-space', H_2 have been investigated by Briggs and co-workers and elegantly generalized to *N*-particle systems [8, 9]. Walter *et al* [9] have formally shown that the HeL approach [4, 5] is the lowest order approximation in the angular momentum expansion of the electron pair wavefunction consistent with homonuclear H_2 (or D_2).

There is currently much effort to solve the full Schrödinger equation for PDI in H_2 within the Born-Oppenheimer approximation. Both the time-dependent close coupling (TDCC) [10, 11] and the exterior complex scaling (ECS) [12-15] methods have been applied to this problem. The calculated FDCSs are extremely sensitive to the correlation between electrons in the molecular ground state, which depends on the internuclear distance of the two protons [13-15], and in the final states, resulting in an outgoing electron pair moving in the Coulomb molecular field [11,13-15].

2. Experimental details

The measurements were performed at the gas phase photoemission beamline of the Elettra synchrotron radiation source operated in four-bunch mode. Our momentum imaging apparatus, CIEL [18, 19], enables the detection of the two electrons and two protons from the Coulomb explosion of H_2 molecules with 4π sr detection efficiency.

The CIEL apparatus comprises two coaxial time-of-flight (TOF) analysers each one fitted with a position-sensitive detector with multi-hit capability [19]. The H_2 molecules are ionised by 100% linearly polarised VUV synchrotron radiation and the resulting charged particles are extracted by a weak static electric field applied across the interaction region with electrons and ions travelling in opposite directions. An axial magnetic field is also applied to confine electrons having a large initial orthogonal velocity component. The (*x,y,t*) information *of all four* ejected particles is obtained for each double ionisation event and directly mapped into the corresponding (p_x,p_y,p_z) components using classical equations of motion [18].

The photon energy was 76.09 eV, i.e. ~25 eV above the nominal threshold at the equilibrium internuclear separation and near the peak maximum of the H_2 double ionisation total cross section. The CIEL apparatus was able to detect electrons from 2 to 23 eV kinetic energy in addition to the two ~10 eV protons. Events with an arrival time difference between particles smaller than ~1.5 ns cannot be disentangled. Since the TOF axis was perpendicular to the polarization direction, the dead time interval results in 'dead' angular sectors that are symmetric with respect to the vertical line in the coplanar geometry figures shown below. The angle and relative energy resolutions were typically 5° and 15%, respectively, for 12.5 eV electrons. We present here a subset of our data corresponding to the FDCSs in the equal electron energy sharing case, $E_1 = E_2 = 12.5$ eV; the unequal energy sharing case will be considered separately.

3. Determination of Absolute Fully Differential Cross Sections for He and H_2

3.1. Helium

In order to determine the *absolute* FDCSs of helium we have used the method reported in [20, 21]. The helium FDCS can be expressed by:

$$\sigma^{(4)} = \frac{d^4\sigma}{d\theta_1 d\theta_2 d\Delta\phi_{12} dE_1}$$

where $\theta_{1,2}$ are the polar angles of electrons 1 and 2 with respect to $\vec{\varepsilon}$, $\Delta\phi_{12} = \phi_1 - \phi_2$ is the relative azimuthal angle, and E_1 is the energy of one electron; the energy of the second electron being determined by energy conservation $h\upsilon = E_1 + E_2 + IP(He^{2+})$. When $\sigma^{(4)}$ is essentially constant in the detection volume $V^{(4)}$, the *absolute* FDCS is connected to the *experimental* FDCS, $\sigma^{(4)}_{\exp}$, via:

$$\sigma^{(4)} \approx \sigma^{(4)}_{\exp} = \frac{\sigma^{2+}_{He}}{N_{tot}} \frac{N^{(4)}}{\int_{V^{(4)}} dV^{(4)}}$$

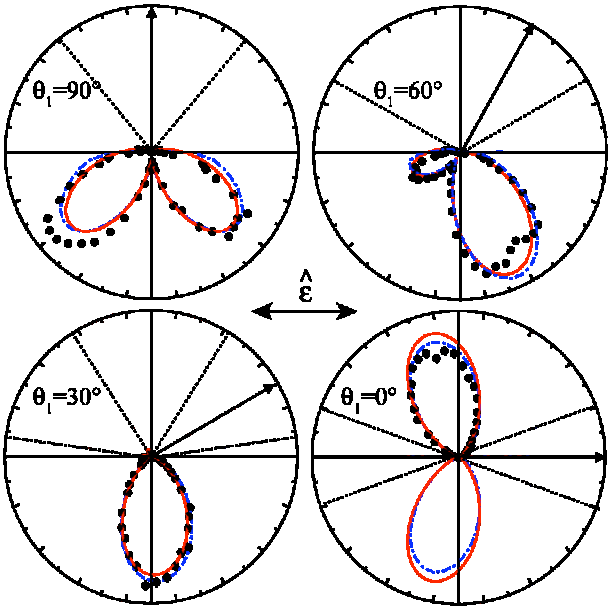

Figure 1. Absolute helium FDCS's in the 'coplanar' geometry ($|\Delta\phi_{12}|$ = 0° or 180°) with electron 1 indicated by the arrow at θ_1 = 90°, 60°, 30°, 0° for E_1= E_2= 12.5±2.5 eV. The radii of the circles give the absolute scales of 30, 30, 25, 10 barns/eV/sr^2 for the four plots respectively. The angular step in θ_2 is 5° for all cases. The thin lines indicate a dead sector, symmetric with respect to the vertical axis, for the detection of the second electron. The angular bandwidths are: ±15°, ±20° for θ_1 and $\Delta\phi_{12}$, respectively. The solid lines (red) show the HRM-*SOW* calculation [23] and the dash-dot lines (blue) represent a fit to the data with an exact parameterization [24], both incorporating experimental bandwidths.

where σ_{He}^{2+} is the integral cross section of 8.76 kBarns at 25 eV above the double ionization threshold [22], N_{tot} the total number of events detected by the experiment, $N^{(4)}$ the number of events within the detection volume and $dV^{(4)}$ the infinitesimal detection volume element. In the dipole approximation, the FDCS has axial symmetry around the polarisation axis, hence $dV^{(4)}$ can be expressed by:

$$dV^{(4)} = \Delta\phi_1 \sin\theta_1 d\theta_1 \sin\theta_2 d\theta_2 d\Delta\phi_{12} dE_1.$$

For the present experimental conditions, the photon energy resolution (~200 meV) is negligible with respect to the electron energy bandwidth ±2.5 eV.

Helium data are presented in figure 1 for the 'coplanar' geometry, i.e. where the electron momenta, $\vec{k}_{1,2}$, and polarization vector, $\vec{\varepsilon}$, all lie in the same plane. Also presented are the results of Hyperspherical *R*-matrix with Semiclassical Outgoing Waves (HRM-*SOW*) [23] calculations (full lines) and the best fit obtained with an exact parameterization (dash-dot lines) [24] taking into account the experimental bandwidths. Excellent agreement between theory and experiment is found, both in magnitude and in shape, for all values of θ_1. The relative differences between the HRM-*SOW* calculation and the parameterization do not exceed 5%, insuring that the fitting procedure converges properly despite some small fluctuations which can be observed in the figure. Note that this parameterization for the cross section of helium at equal sharing is given by $|a_g|^2(\cos\theta_1 + \cos\theta_2)^2$, with a single amplitude, a_g, that is often approximated by a Gaussian function:

$$|a_g|^2 \propto \exp\left(-4\ln(2)(180 - \theta_{12})^2 / \theta_{1/2}^2\right)$$

where the correlation half-width, $\theta_{1/2}$ depends solely on the excess energy, $E = E_1 + E_2$. This functional form gives remarkably accurate shapes for a wide range of *E;* the width found at this excess energy is 90 ± 3° in good agreement with previous studies, e.g. see [20]. Clearly the normalization procedure applied to helium PDI at this photon energy achieves a high level of accuracy.

3.2. Hydrogen

For hydrogen we have extended the above method by taking into account the molecular orientation and that the energy of the second electron must satisfy energy conservation, i.e.:

$$h\upsilon = E_1 + E_2 + 2(IP(H^+) + E_N)$$

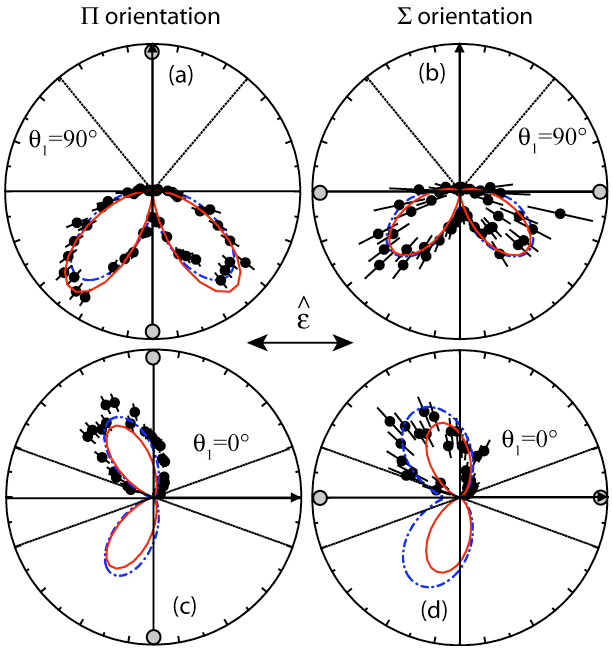

Figure 2. Absolute H_2 FDCS's in the 'coplanar' geometry for four different orientations of the molecule and the fixed electron. The angular bandwidths are: ±15° for θ_1 (a,b), ±20° for θ_1 (c,d); ±20° for $\Delta\phi_{12}$ (a,b, not relevant in b,d); ±20° for θ_N (a,c), ±30° for θ_N (b,d); ± 45° for $\Delta\phi_{1N}$ (a), ± 45° for $\Delta\phi_{2N}$ (c), not relevant in cases (b,d). The angular step in θ_2 is 5° in all cases. In (c) and (d) only one lobe is reported. The radii of the circles give the absolute scales of 120; 50; 40; 20 millibarns/eV^2/sr^3. The solid lines (red) give the HeL shape without integration and the dash-dot lines (blue) is the fit using this model and taking into account experimental solid angles [3].

where E_N is the kinetic energy of one proton and $IP(H^+)$ is the ionization potential of the hydrogen atom. Hence, the FDCS can be reformulated as:

$$\sigma^{(7)} = \frac{d^7\sigma}{d\theta_1 d\theta_2 d\Delta\phi_{12} d\theta_N d\Delta\phi_{eN} dE_1 dE_2}$$

where θ_N is the polar angle of the molecular axis, N, with respect to $\hat{\varepsilon}$, and where $\Delta\phi_{eN} = \phi_e - \phi_N$ (with e = 1 or 2) are the relative azimuthal angles with respect to one electron. As in the helium case, the *absolute* FDCS, $\sigma^{(7)}$, is connected to the *experimental* FDCS, $\sigma^{(7)}_{\text{exp}}$ by:

$$\sigma^{(7)} \approx \sigma^{(7)}_{\text{exp}} = \frac{\sigma^{2+}_{H_2}}{N_{tot}} \frac{N^{(7)}}{\int_{V^{(7)}} dV^{(7)}}$$

with $dV^{(7)} = \Delta\phi_1 \sin\theta_1 d\theta_1 \sin\theta_2 d\theta_2 \sin\theta_N d\theta_N d\Delta\phi_{12} d\Delta\phi_{eN} dE_1 dE_2$. The integral cross section, $\sigma^{2+}_{H_2}$, is 2.5 kBarns at 25 eV above threshold [25].

At this excess energy and for equal energy sharing, the *velocity* of the electrons is much higher than those of the two ions, thus the molecule can be considered as 'fixed in space'. Furthermore, since the asymptotic de Broglie wavelengths are larger than the internuclear separation, we can infer that the molecule is essentially viewed as an atom by the out-going electron pair. So it is not inappropriate to discuss the data in terms of the HeL model, where the form of the FDCS for equal electron energy sharing ($E_1 = E_2$) is given by:

$$\sigma^{(7)} = \left| \begin{array}{l} \left(a_\Sigma \cos^2\theta_N + a_\Pi \sin^2\theta_N\right)\left(\cos\theta_1 + \cos\theta_2\right) \\ +\left(a_\Sigma - a_\Pi\right)\sin\theta_N \cos\theta_N \left(\sin\theta_1 \cos\left(\phi_1 - \phi_N\right) + \sin\theta_2 \cos\left(\phi_2 - \phi_N\right)\right) \end{array} \right|^2$$

a_Σ and a_Π are complex transition amplitudes which depend only on the energies E_1, E_2 and the mutual angle θ_{12} of the two electrons. These amplitudes respectively account for the PDI process when the molecule is oriented parallel or perpendicular to the polarisation axis. They can be approximated in a HeL description by a simple Gaussian function. For intermediate orientations, the two Σ and Π terms are mixed coherently depending only on the angles θ_N, ϕ_N.

We have successfully extracted all parameters with a least squares fitting procedure of the whole 3-dimension $E_1 = E_2$ coplanar data set taking into account the detection solid angles of the

experiment [3]. In figure 2, we consider the consequence of the integration over experimental solid angles for the most sensitive geometries $\theta_1 = 90°$ and $\theta_1 = 0°$ and the two Σ and Π orientations.

In all cases, the integration over experimental solid angles (dash-dot lines) produces minor changes on the shape of the HeL FDCS (full lines). A general feature is that the back-to-back node is partially filled, as previously discussed [26]. For $\theta_1 = 90°$ and the Π molecular orientation, the yield ($\int \sigma^{(7)} d\theta_2$) is at its maximum, the integration over experimental solid angles changes by not more than 12% the lobe intensity. In the situation, where $\theta_1 = 0°$ and the Σ molecular orientation, the yield ($\int \sigma^{(7)} d\theta_2$) reaches its minimum and a 20% deviation of the lobe intensity is observed when the integration is performed. For this special case, one should note that the shape is slightly modified resulting in an apparent broadening of the lobes with a closer opening angle. However, the variation of the cross section is rather small. It is thus reasonable to assume that integration introduces a minor uncertainty in the determination of the *absolute* FDCS.

Within the HeL formalism [5], there is a connection between the $|a_\Pi / a_\Sigma|$ value and the ion asymmetry parameter β_N, namely:

$$\beta_N = \frac{2(1 - |a_\Pi / a_\Sigma|^2)}{1 + 2|a_\Pi / a_\Sigma|^2}$$

This naturally gives a self-consistent check of the reliability of the deduced parameters. We found a value $|a_\Pi / a_\Sigma|$ = 2.25 ± 0.35 which gives $\beta_N \approx$ -0.73 ± 0.1. This is consistent with previous ion measurements yielding $\beta_N \approx$ -0.68 ± 0.04 for E = 25 eV [25] and supports the ratio observed between the two Σ and Π orientations.

One can also remark that the change in magnitude between $\theta_1 = 90°$ and $\theta_1 = 0°$ is well reproduced by the HeL model assuming Gaussian distributions for the amplitudes with $\theta_{1/2}^{\Pi} = 73 \pm 2°$ and $\theta_{1/2}^{\Sigma} = 93° \pm 4°$. For the presented geometries, the yield is related to the product of dynamical and kinematical factors, which reduces to an exact $\left|a_{\Sigma,\Pi}\left(\cos\theta_1 + \cos\theta_2\right)\right|^2$ dependence for (Σ, Π) orientations, respectively. The maxima of the FDCSs at $\theta_1 = 90°$ and 0° thus strongly depend on the correlation half-widths $\theta_{1/2}^{\Sigma,\Pi}$ of the amplitudes.

4. Comparison with TDCC calculations

The first step toward a precise quantum mechanical solution of the molecular PDI problem was reached a few years ago using a grid-base time-dependent close-coupling (TDCC [10]) and exterior complex scaling (ECS [12]) methods. Both methods assume the Born-Oppenheimer approximation and led to extended calculations that where able to produce both integral and differential cross sections [10-15]. However, as the internuclear separation R is fixed, the absolute FDCS requires an arbitrary scaling factor. In the TDCC method all possible outgoing energies and angles of both electrons and ions are produced by a single calculation at a given photon energy. Consequently, integration over experimental solid angles and energy bandwidths can be easily performed.

In figure 3 the experimental data are compared to recent TDCC [11] calculations (full lines) in the 'coplanar' geometry, where the momenta, $\vec{k}_{1,2,N}$ and the polarization vector, $\vec{\varepsilon}$, all lie in the same plane. We consider only the FDCSs for θ_1 = 90° and 0° in two molecular orientations (Σ, Π), as these geometries represent the most stringent test for the theory.

The FDCSs have a characteristic symmetrical two-lobe structure very similar to that observed in helium with $E_1 = E_2$ at the same θ_1 angle. Coulomb repulsion between the electrons is responsible for the overall tendency for the electrons to be in the opposite hemisphere with a quantum mechanical node for 'back-to-back' emission. In general, the agreement between the TDCC calculations and the measurements is good in terms of the FDCS *shape*. Significant changes in FDCS magnitudes are observed experimentally between Σ and Π orientations. This trend is even more pronounced in the

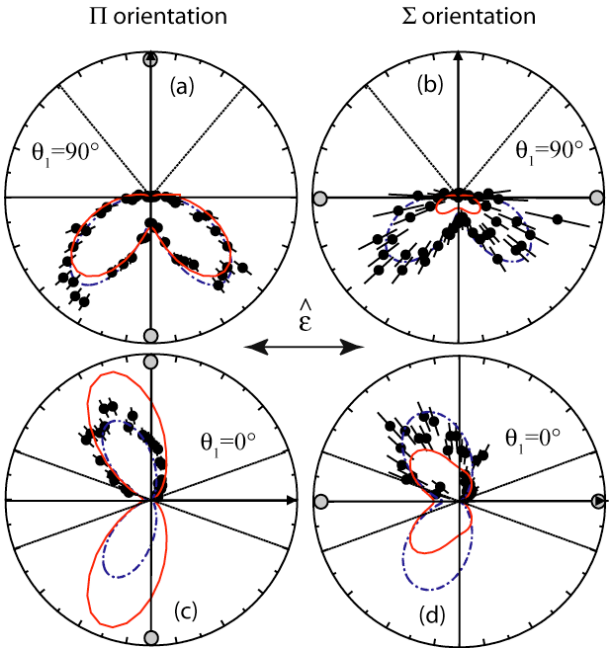

Figure 3. Absolute H_2 FDCS's in the 'coplanar' geometry for four 'in plane' molecular orientations (see caption figure 2). The radii of the circles give the absolute scales of 120; 50; 40; 20 millibarns/eV^2/sr^3. The full (red) lines are the TDCC calculation [11] and the (blue) dash-dot lines are the HeL model [3] (both curves incorporate experimental bandwidths).

TDCC results shown in figure 3, which are integrated over the experimental electron energy and angular bandwidths. This difference may be related to a larger (i.e. more negative) β_N parameter in the calculation than observed and/or significant variation in $\sigma^{(7)}$ when the molecular orientation changes close to the polarization axis. An interesting feature can be noticed for a fixed molecular orientation while the angle of the fixed electron varies from $\theta_1 = 90°$ to 0°. The intensities of the FDCSs vary less in TDCC than in the data for both Π and Σ orientations. In the Σ orientation the TDCC FDCSs hardly change in magnitude while the experimental results reduce by a factor 3.

A striking effect can be observed at another geometry, where pronounced changes of the observed FDCS depart from the HeL model [3]. Data, where $\vec{k}_1$ is perpendicular to the plane containing $\vec{k}_2,\vec{\varepsilon}$, are reported along with the TDCC theoretical calculation in figure 4. In this 'orthogonal' geometry, the electron-electron mutual angle, θ_{12}, is a constant 90°; consequently the electron correlation aspect is "frozen", in contrast with coplanar geometry. The angular distributions thus probe the partial wave expansion of the outgoing electron. Note that the electronic correlation in the initial state strongly affects this partial wave expansion.

Due to Coulomb repulsion, the FDCS in the orthogonal geometry is much smaller than in the coplanar geometry. The integration over experimental solid angles is therefore very sensitive. In the present case, experiment and theory achieve remarkable agreement in shape, although there is a scaling factor of 2.2 in the Σ orientation. Experimental data and theoretical calculations support that the three orientations shown in figure 4 differ from each other, while they are equivalent in the HeL model [3]. Where the HeL model fails to explain the observed effects a precise quantum treatment clearly reproduces the observation. This difference is not so surprising since only the projection of angular momentum onto the nuclear axis is conserved in the molecular case, and the outgoing pair may have higher angular momentum than assumed in the HeL model. It is likely that the exact approach [9] using generalized shape coordinates for the H_2 system could shed some light on the present observations.

5. Role of nuclear motion

In the orthogonal geometry, Weber *et al* [1] found marked differences in the angular patterns of ejection of the electrons with changes in the nuclear momenta. This observation, attributed to changes of electron correlation in the ground state with internuclear distance, has recently been supported by

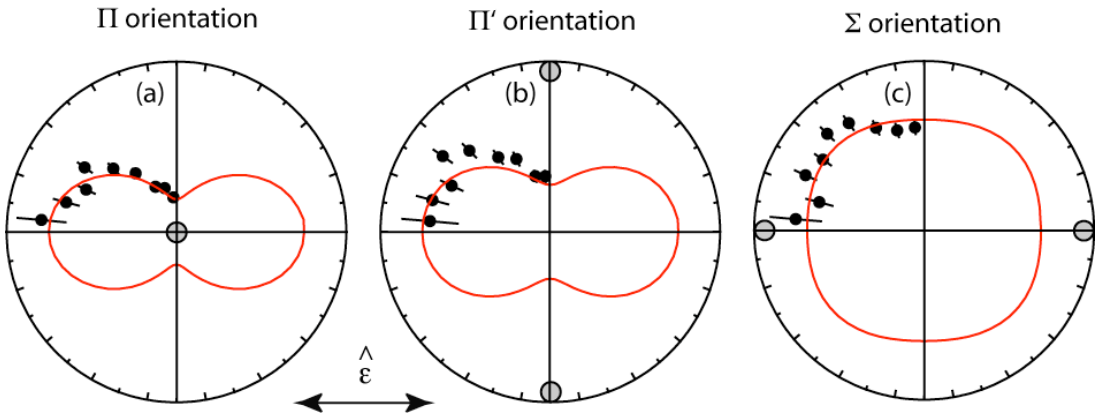

Figure 4. Absolute H_2 FDCSs for $E_1 = E_2 = 12.5 \pm 4$ eV in the 'orthogonal' geometry with one electron at $\theta_1 = 90°$, perpendicular to the plane of the figure, which contains the second electron ($|\Delta\phi_{12}| = 90°$ or 270°). The molecule is oriented: (a) perpendicular to this plane ($|\Delta\phi_{1N}| = 0°$or 180°), and (b,c) in this plane ($|\Delta\phi_{1N}| = 90°$or 270° for (b); not relevant for (c)). The four quadrants are related by symmetries and equivalent data have been added. The absolute scale is given by their maxima at 22, 14, 14 millibarns/eV^2/sr^3. The angular bandwidths are: ±20° for θ_1 (a,b), ±30° for θ_1 (c); ±20° for $\Delta\phi_{12}$; ±25° for θ_N (a,b), ±30° for θ_N (c); ±45° for $\Delta\phi_{1N}$ (a,b, not relevant for c). The full lines are the TDCC theoretical results integrated over experimental bandwidths.

theory [12-15]. Horner *et al* [15] suggested that this observation is due to the interference between the Σ and Π orientations and the subsequent change in the relative contributions of the two amplitudes in PDI for various internuclear distances. The dynamical effects found in the 'orthogonal' geometry clearly highlight the change in the partial wave expansion but they cannot probe what happens when the mutual angle between the electrons varies.

Figure 5 reveals the presence of such dynamical effects for equal sharing energy in the *coplanar* geometry in the Σ orientation. The value of R is selected experimentally by choosing the proton kinetic energy, E_N, and using the reflection principle. The two lobes are clearly closer together (i.e. further away from the direction of the reference electron) at shorter internuclear distance ($<R> = 1.2$ a.u.) than at $<R> = 1.6$ a.u., which is indicative of a greater degree of electron correlation. This change of the degree of correlation may be connected to the ground state molecular orbitals, which are more localized to the proton when the molecule is stretched than when compressed. No evidence of these dynamical effects has been observed in the vicinity of Π orientation. The electron correlation appears to be stronger in the Π orientation than in the Σ orientation [3], i.e. $\theta_{1/2}^{\Pi} < \theta_{1/2}^{\Sigma}$ in terms of the HeL model. Thus a tentative explanation can be given: close to Π orientation, the final state correlation masks the change of the initial state with the internuclear separation, which survives only close to Σ orientation. In any case our observations show that the effects of nuclear dynamics are prominent close to Σ orientation. These phenomena are not yet well understood, and they appeal for more theoretical work, using for instance the already mentioned approach [9].

In summary the reported analysis, restricted to equal energy sharing, has been focused on the effect of changing the molecular orientation, from Π toΣ, on the electron angular distributions. Further investigation with unequal energy sharing, including the role of the internuclear separation, is in progress.

We would like to thank the staff at Elettra and the Gas Phase beamline team for their invaluable assistance, and EU, NSERC and UoW for their financial support. We thank J. Colgan, L. Malegat and P. Selles for providing us their numerical data and for useful discussions.

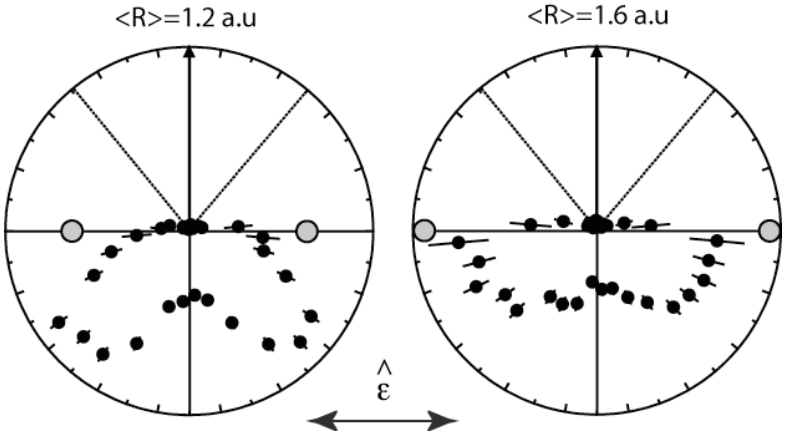

Figure 5. FDCSs for H_2 (a.u.) for $E_1 = E_2 = 12.5 \pm 10$ eV in the 'coplanar' geometry with one electron at $\theta_1 = 90°$ and the molecule is in Σ orientation; the angular bandwidths are: ±15° for θ_1; ±30° for $\Delta\phi_{12}$; ±40° for θ_N ; $\Delta\phi_{1N}$ and $\Delta\phi_{2N}$ are not relevant.

References

[1] Weber T *et al* 2004 *Nature* **431** 437; Weber T *et al* 2006 *Nature* **443** 1014
[2] Weber T *et al* 2004 *Phys Rev Letts* **92** 163001
[3] Gisselbrecht M, Lavollée M, Huetz A, Bolognesi P, Avaldi L, Seccombe D P, Reddish T J 2006 *Phys. Rev. Lett.* **96** 153002
[4] Feagin JM 1998 *J. Phys. B: At. Mol. Opt. Phys.* **31** L729
[5] Reddish TJ and Feagin JM 1999 *J. Phys. B: At. Mol. Opt. Phys.* **32** 2473
[6] Kheifets AS 2005 *Phys. Rev. A.* **71** 022704
[7] Kheifets AS and Bray I 2005 *Phys Rev A* **72** 022703
[8] Walter M and Briggs JS 2000 *Phys. Rev. Lett.* **85** 1630
[9] Walter M, Meremianin A and Briggs JS 2003 *J. Phys. B: At. Mol. Opt. Phys.* **36** 4561
[10] Colgan J, Pindzola MS, and Robicheaux F 2004 *J. Phys. B: At. Mol. Opt. Phys.* **37** L377
[11] Colgan J, Pindzola MS and Robicheaux F 2007 *Phys. Rev. Lett.* **98** 153001
[12] Vanroose W, Martín F, Rescigno T N and McCurdy CW 2004 *Phys Rev A* **70** 050703
[13] Vanroose W, Martín F, Rescigno T N and McCurdy CW 2005 *Science* **310** 1787; Vanroose W 2006 *Science* **314** 254
[14] Vanroose W, Horner DA, Martín F, Rescigno TN and McCurdy W 2006 *Phys. Rev. A* **74** 052702
[15] Horner DA, Vanroose W, Martín F, Rescigno TN and McCurdy CW 2007 *Phys. Rev. Lett.* **98** 073001
[16] Zare RN 1972 *Mol Photochem* **4** 1
[17] Avaldi L and Huetz A 2005 *J. Phys. B: At. Mol. Opt. Phys.* **38** S861 *and references therein*
[18] Gisselbrecht M, Huetz A, Lavollée M, Reddish TJ and Seccombe DP 2005 *Rev Sci Instrum* **76** 013105
[19] Lavollée M 1999 *Rev. Sci. Instrum.* **70** 2968
[20] Bräuning H *et al* 1998 *J. Phys. B. At. Mol. Opt. Phys* **31** 5149
[21] Bouri C, Selles P, Malegat L and Kwato Njock MG 2006 *Phys. Rev. A* **73** 022724
[22] Samson JAR, Stolte WC, He ZX, Cutler JN, Lu Y and Bartlett RJ 1998 *Phys. Rev.* A **57** 1906
[23] Selles P ,Malegat L and Kazansky A K 2002 *Phys. Rev. A* **65** 032741 and priv. comm.
[24] Huetz A, Selles P, Waymel P and Mazeau J 1991 *J. Phys. B: At. Mol. Opt. Phys.* **24** 1917
[25] Kossmann H, Schwarzkopf O, Kämmerling B and Schmidt V 1989 *Phys. Rev. Lett.* **63**, 2040
[26] Seccombe DP, Collins SA, Reddish TJ, Selles P, Malegat L, Kazansky AK and Huetz A 2002 *J. Phys. B: At. Mol. Opt. Phys.* **35** 3767